

Suppression of the nuclear rainbow in the inelastic nucleus-nucleus scattering

Nguyen Hoang Phuc¹, Dao T. Khoa¹, Nguyen Tri Toan Phuc^{1,2}, and Do Cong Cuong¹

¹ Institute for Nuclear Science and Technology, VINATOM
179 Hoang Quoc Viet, Cau Giay, 100000 Hanoi, Vietnam

² Department of Nuclear Physics, University of Science, VNU-HCM
227 Nguyen Van Cu, District 5, 700000 Ho Chi Minh City, Vietnam

Received: date / Revised version: date

Abstract. The nuclear rainbow observed in the elastic α -nucleus and light heavy-ion scattering is proven to be due to the refraction of the scattering wave by a deep, attractive real optical potential. The nuclear rainbow pattern, established as a broad oscillation of the Airy minima in the elastic cross section, originates from an interference of the refracted far-side scattering amplitudes. It is natural to expect a similar rainbow pattern also in the inelastic scattering of a nucleus-nucleus system that exhibits a pronounced rainbow pattern in the elastic channel. Although some feature of the nuclear rainbow in the inelastic nucleus-nucleus scattering was observed in experiment, the measured inelastic cross sections exhibit much weaker rainbow pattern, where the Airy oscillation is suppressed and smeared out. To investigate this effect, a novel method of the near-far decomposition of the inelastic scattering amplitude is proposed to explicitly reveal the coupled partial-wave contributions to the inelastic cross section. Using the new decomposition method, our coupled channel analysis of the elastic and inelastic $^{12}\text{C}+^{12}\text{C}$ and $^{16}\text{O}+^{12}\text{C}$ scattering at the refractive energies shows unambiguously that the suppression of the nuclear rainbow pattern in the inelastic scattering cross section is caused by a destructive interference of the partial waves of different multipoles. However, the inelastic scattering remains strongly refractive in these cases, where the far-side scattering is dominant at medium and large angles like that observed in the elastic scattering.

PACS. 24.10.Ht Optical and diffraction models – 25.55.Ci Elastic and inelastic scattering – 25.70.Bc Elastic and quasielastic scattering

1 Introduction

The optical model (OM) studies of elastic heavy-ion (HI) scattering usually shows a strong absorption that suppresses the refractive (large-angle) scattering, and elastic HI scattering occurs mainly at the surface. However, with the nuclear rainbow pattern observed in the elastic scattering of some α -nucleus and light HI systems, the absorption turns out to be much weaker and the refractive, far-side scattering becomes dominant at medium and large angles [1, 2, 3]. Not only a fascinating semiclassical analog to the atmospheric rainbow, the nuclear rainbow also enables the determination of the real nucleus-nucleus optical potential (OP) with much less ambiguity, down to small internuclear distances [3]. The pattern of the nuclear rainbow is usually characterized by a broad oscillation of the Airy minima [1, 2, 3] in the elastic cross section. The observation of these minima, especially, the first Airy minimum A1 that is followed by a broad shoulder-like maximum, not only facilitates the determination of the real OP but also provides an useful probe of the cluster structure of light nuclei [4, 5].

Similarly to the atmospheric rainbow, the nuclear rainbow can be interpreted as a pattern resulted from an interference of the two scattering amplitudes, as shown by the barrier-wave/internal-wave (BI) or near-side/far-side (NF) decomposition of the elastic scattering amplitude. The BI method proposed by Brink and Takigawa [6] describes elastic HI scattering in terms of the internal waves penetrating through the potential barrier into the nuclear interior, and barrier waves reflected from the barrier. On the other hand, the NF decomposition suggested by Fuller [7] splits the elastic scattering amplitude into the near-side (N) and far-side (F) components, corresponding to the waves deflected to the near side and far side of the scattering center, respectively. These two interpretations are complementary, and the broad Airy oscillation of the nuclear rainbow pattern is given by the interference of two far-side amplitudes [3, 8, 9, 10]. These are either the barrier f_{BF} and internal f_{IF} far-side amplitudes [6], or $f_{\text{F} <}$ and $f_{\text{F} >}$ far-side amplitudes with the orbital momenta L smaller or larger than a critical value L_{R} associated with the rainbow angle θ_{R} [7].

From such a pattern of the nuclear rainbow, a similar Airy structure is expected to be seen also in the inelastic scattering of a light HI or α -nucleus system that shows a strong rainbow pattern in the elastic scattering. In fact, some feature of the nuclear rainbow was observed in the inelastic light HI scattering [11, 12, 13, 14, 15, 16, 17, 18, 19, 20], and some of these data were analyzed using the BI [14] and NF [17, 18, 19, 20] decomposition methods. Although these studies have confirmed the dominance of the far-side scattering at large angles, the Airy oscillation pattern could not be clearly identified in the inelastic cross section. Such suppression of the nuclear rainbow was assumed by

scattering data were proven to be strongly refractive, with the first Airy minimum A1 followed by a broad rainbow shoulder [24], especially, in the elastic $^{16}\text{O}+^{12}\text{C}$ scattering data at 200 MeV shown in the lower panel of Fig. 1. While the cross section of the inelastic scattering to the 2_1^+ state of ^{12}C target is quite strong, A1 disappears in the inelastic cross section and the Airy pattern is smeared out. The measured inelastic scattering cross section of the 2_1^+ state is even larger than the elastic scattering cross section at medium and large angles, which confirms that the inelastic scattering channel remains strongly refractive. Thus, the disappearance of the Airy pattern should not be due to an enhanced absorption in the exit 2_1^+ channel.

To explore this effect, we propose a compact method for the NF decomposition of the inelastic scattering amplitude to determine explicitly all partial wave contributions to the angular momentum transfer to the spin of the excited target. For this purpose, the NF decomposition method by Fuller [7] is extended to split the inelastic scattering amplitude of the coupled partial waves into the near-side and far-side components, so that the refraction in the inelastic scattering channel is studied on equal footing with that in the elastic channel, and the formation of the nuclear rainbow therein. Given the prominent nuclear rainbow pattern observed in the elastic $^{12}\text{C}+^{12}\text{C}$ and $^{16}\text{O}+^{12}\text{C}$ scattering at the refractive energies around 10 ~ 20 MeV/nucleon, we apply the extended NF decomposition method to the inelastic scattering to the 2_1^+ (4.44 MeV) state of ^{12}C target in the coupled channel (CC) analysis of the inelastic scattering data measured for the $^{12}\text{C}+^{12}\text{C}$ system at $E_{\text{lab}} = 240$ MeV [21, 22], and the $^{16}\text{O}+^{12}\text{C}$ system at $E_{\text{lab}} = 200$ and 260 MeV [16, 23].

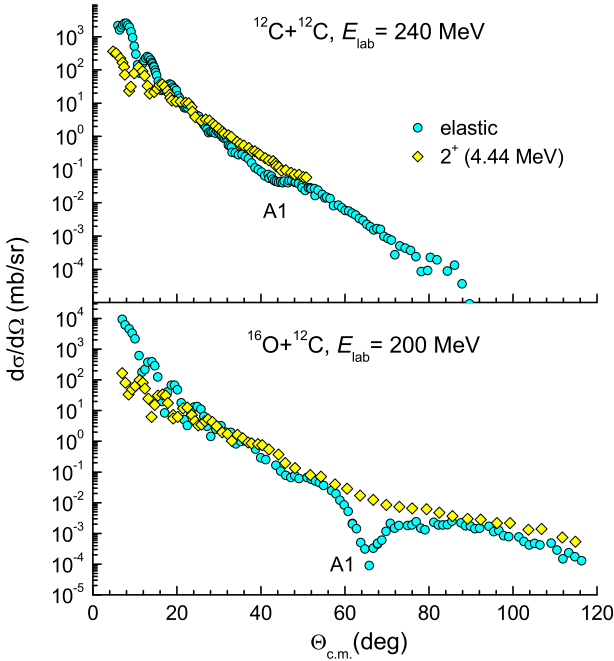


Fig. 1. Angular distributions of the elastic scattering and inelastic scattering to the 2_1^+ state of ^{12}C measured for the $^{12}\text{C}+^{12}\text{C}$ system at $E_{\text{lab}} = 240$ MeV [21, 22] (upper part) and $^{16}\text{O}+^{12}\text{C}$ system at $E_{\text{lab}} = 200$ MeV [16, 23] (lower part). A1 indicates the location of the first Airy minimum established in the extended OM analysis [24] of the elastic scattering data.

Khoa *et al.* [13] to be due to the increased absorption in the exit channel, with the target nucleus in an excited state. Dem'yanova *et al.* [18] suggested that this effect is linked to the shape of the inelastic form factor, which is different from that of the attractive, deep real OP. We note that the inelastic scattering to the 0_2^+ state of ^{12}C (Hoyle state) seems to exhibit the same rainbow pattern as that seen in the elastic scattering cross section, and Hamada *et al.* [15] suggested that this is due to the extended 3α -cluster structure of the Hoyle state.

The weakening or suppression of the Airy oscillation in the inelastic nucleus-nucleus scattering remains so far an unsolved problem. As an illustration, we show in Fig. 1 the elastic and inelastic scattering data measured for the $^{12}\text{C}+^{12}\text{C}$ system at $E_{\text{lab}} = 240$ MeV [21, 22] and for the $^{16}\text{O}+^{12}\text{C}$ system at $E_{\text{lab}} = 200$ MeV [16, 23]. These elastic

2 Near-far decomposition of the inelastic scattering amplitude in the CC formalism

2.1 General formalism

We recall here briefly the coupled channel equations for the elastic and inelastic nucleus-nucleus scattering. The scattering wave function is obtained at each total angular momentum J^π of the nucleus-nucleus system from the solution of the following CC equations [25]

$$\left\{ \frac{\hbar^2}{2\mu_\beta} \left[\frac{d^2}{dR^2} + k^2 - \frac{L(L+1)}{R^2} \right] - \langle \beta(LI)J | V | \beta(LI)J \rangle \right\} \times \chi_{\beta J}(k, R) = \sum_{\beta' L' I'} \langle \beta(LI)J | V | \beta'(L'I')J \rangle \chi_{\beta' J}(k', R), \quad (1)$$

where β and β' denote the entrance and exit channels, respectively; μ_β is the reduced mass, $\hbar k = \sqrt{2\mu_\beta E_\beta}$ is the center-of-mass (c.m.) momentum, and $\chi_{\beta J}(k, R)$ is the scattering wave function at the internuclear radius R . The total angular momentum J is determined from the spin I (I') and orbital momentum L (L') of the entrance (exit) channel by the angular momentum addition $\mathbf{J} = \mathbf{L} + \mathbf{I} = \mathbf{L}' + \mathbf{I}'$. In the present work, we focus on the scattering of the two spinless nuclei ($I = 0$) with a natural-parity

excitation of the target. Then, $|L' - I'| \leq J = L \leq L' + I'$, where I' is the spin of the excited target.

The diagonal matrix element $V_{\beta\beta}(R)$ of the projectile-target interaction in Eq. (1) is the nucleus-nucleus OP, and the nondiagonal matrix element $V_{\beta\beta'}(R)$ is the transition potential, which is also dubbed as the inelastic scattering form factor (FF). The OP and inelastic scattering FF can be evaluated microscopically in the double-folding model (DFM) using the ground-state (g.s.) and transition nuclear densities, respectively, and an effective nucleon-nucleon (NN) interaction between the projectile- and target nucleons (see more details in Ref. [25]). From the solution of the CC equations (1), we obtain the elastic scattering amplitude as

$$f(\theta) = f_C(\theta) + \frac{1}{2ik} \sum_L (2L+1) \exp(2i\sigma_L) (S_L - 1) P_L(\cos\theta), \quad (2)$$

where $f_C(\theta)$ and σ_L are the Rutherford scattering amplitude and Coulomb phase shift, respectively; S_L is the diagonal element of the elastic scattering S matrix, and $P_L(\cos\theta) \equiv P_{LM=0}(\cos\theta)$ is the Legendre function of the first kind. Within the CC formalism [26], the amplitude of the inelastic scattering to an excited state of the target with spin I' and projection $M_{I'}$ is written explicitly as

$$f_{M_{I'}}(\theta, \phi) = \frac{\sqrt{4\pi}}{2ik} \sum_{L, L'} \sqrt{2L+1} \langle L' - M_{I'} I' M_{I'} | L 0 \rangle \times \exp[i(\sigma_L + \sigma'_{L'})] S'_{L'L} Y_{L'-M_{I'}}(\theta, \phi). \quad (3)$$

Here $Y_{LM}(\theta, \phi)$ is the spherical harmonics, the Coulomb phase shift $\sigma'_{L'}$ is evaluated from the c.m. momentum k' in the exit channel, and $S'_{L'L}$ is the element of the inelastic scattering S matrix. The orbital angular momenta in the entrance and exit channels are linked with spin I' of the excited target by the triangular rule

$$L' = L - I', L - I' + 2, \dots, L + I' - 2, L + I', \quad (4)$$

where the step of two angular-momentum units is implied by the parity conservation.

2.2 Multipole mixing of the partial waves

One can see from the expansion (3) that the coupled partial waves of different multiplicities can contribute coherently to the inelastic scattering amplitude at the same scattering angle θ when $I' \neq 0$. By expressing the selection rule (4) as $L' = L + K$, the inelastic scattering amplitude (3) can be written in terms of the K -subamplitudes allowed by the selection rule (4)

$$f_{M_{I'}}(\theta, \phi) = \sum_{K=-I'}^{I'} f_{M_{I'}}^{(K)}(\theta, \phi). \quad (5)$$

Like the elastic amplitude (2), each K -subamplitude of $f_{M_{I'}}(\theta, \phi)$ can be expanded over the orbital momenta of

the entrance channel L as

$$f_{M_{I'}}^{(K)}(\theta) = \frac{\sqrt{4\pi}}{2ik} \sum_L \sqrt{2L+1} \langle (L+K) - M_{I'} I' M_{I'} | L 0 \rangle \times \exp[i(\sigma_L + \sigma'_{L+K})] S'_{(L+K)L} Y_{(L+K)-M_{I'}}(\theta, \phi). \quad (6)$$

In terms of the inelastic scattering cross section, the contribution from each K -subamplitude is obtained at the given scattering angle as

$$\frac{d\sigma_K}{d\Omega} = \sum_{M_{I'}} \left| f_{M_{I'}}^{(K)}(\theta, \phi) \right|^2, \quad (7)$$

so that the full cross section of the inelastic scattering to an excited state of the target with spin I' is

$$\frac{d\sigma}{d\Omega} = \sum_{M_{I'}} \left| \sum_{K=-I'}^{I'} f_{M_{I'}}^{(K)}(\theta, \phi) \right|^2. \quad (8)$$

Thus, for an excited state with spin $I' \neq 0$, the full inelastic scattering cross section is given by the interference of the K -subamplitudes with $K = -I', I' + 2, \dots, I' - 2, I'$.

2.3 Near-far decomposition of the scattering amplitude

As mentioned above, the NF decomposition method by Fuller [7] is a very helpful tool to analyze the interference of the near-side and far-side scattering amplitudes in the elastic scattering [2,3]. Namely, the elastic scattering amplitude is decomposed into the near-side (f_N) and far-side (f_F) components as

$$f(\theta) = f_N(\theta) + f_F(\theta) = f_C^N(\theta) + f_C^F(\theta) + \frac{1}{2ik} \sum_L (2L+1) \exp(2i\sigma_L) (S_L - 1) \times \left[\tilde{Q}_L^{(-)}(\cos\theta) + \tilde{Q}_L^{(+)}(\cos\theta) \right], \quad (9)$$

where $f_C^{N(F)}(\theta)$ is the near-side (far-side) component of the Rutherford scattering amplitude [7], the relative strength of the near-side and far-side nuclear scattering is given by $\tilde{Q}_L^{(-)}(\cos\theta)$ and $\tilde{Q}_L^{(+)}(\cos\theta)$, respectively,

$$\tilde{Q}_L^{(\mp)}(\cos\theta) = \frac{1}{2} \left[P_L(\cos\theta) \pm \frac{2i}{\pi} Q_L(\cos\theta) \right], \quad (10)$$

where $Q_L(\cos\theta) \equiv Q_{LM=0}(\cos\theta)$ is the Legendre function of the second kind. It is well established [2,3,27] that the nuclear rainbow pattern observed in the elastic α -nucleus and light HI scattering is determined entirely by the far-side component of the elastic amplitude (9). The nuclear rainbow pattern is a broad oscillation of the Airy minima at medium and large scattering angles that results from an interference between $f_{F<}(\theta)$ and $f_{F>}(\theta)$ subamplitudes of the far-side component in (9), with L being smaller or larger than a critical partial wave L_R associated with the rainbow angle θ_R [27].

It is natural to expect a similar rainbow pattern also in the inelastic scattering cross section of a nucleus-nucleus system that exhibits a pronounced nuclear rainbow in the elastic scattering channel. For this purpose, a NF decomposition of the inelastic scattering amplitude (3) should be done for each projection $M_{I'}$ of the target spin I' , with the contributions of all allowed K -subamplitudes (6) treated explicitly. However, such a detailed decomposition method is so far unavailable, and only some general discussion on possible Airy structure of the inelastic scattering cross section was made [15,16] based on the Airy pattern established in the elastic scattering cross section. We note here an early attempt to extend the NF decomposition method to the inelastic HI scattering by Dean and Rowley [28], where the near-side and far-side scattering amplitudes obtained for each $M_{I'}$ magnetic substate of the target excitation with $I' \neq 0$ were shown to be *not* in phase. However, the refractive Airy pattern of the nuclear rainbow was not discussed at all in Ref. [28]. To close this gap of the scattering theory, we suggest in the present work a method of the NF decomposition of the inelastic scattering amplitude (3) to investigate explicitly the Airy oscillation pattern in the inelastic scattering cross section. Thus, the NF decomposition (9) is generalized to decompose the inelastic scattering amplitude (3) using the associated Legendre functions as

$$\begin{aligned} f_{M_{I'}}(\theta, \phi) &= f_{M_{I'}}^N(\theta, \phi) + f_{M_{I'}}^F(\theta, \phi) \\ &= \frac{\sqrt{4\pi}}{2ik} \sum_{LL'} \sqrt{2L+1} \langle L' - M_{I'} I' M_{I'} | L0 \rangle \\ &\times A_{L'M_{I'}} \exp[i(\sigma_L + \sigma'_{L'})] \exp(-iM_{I'}\phi) \\ &\times S'_{L'L} \left[\tilde{Q}_{L'-M_{I'}}^{(-)}(\cos\theta) + \tilde{Q}_{L'-M_{I'}}^{(+)}(\cos\theta) \right]. \quad (11) \end{aligned}$$

where $\tilde{Q}_{LM}^{(\mp)}(\cos\theta) = \frac{1}{2} \left[P_{LM}(\cos\theta) \pm \frac{2i}{\pi} Q_{LM}(\cos\theta) \right]$,

$$\text{and } A_{LM} = \sqrt{\frac{2L+1}{4\pi} \frac{(L+M)!}{(L-M)!}}.$$

Here $P_{LM}(\cos\theta)$ and $Q_{LM}(\cos\theta)$ are the associated Legendre functions of the first- and second kind, respectively. We note that the inelastic scattering FF includes both the Coulomb and nuclear contributions [25], and the inelastic Coulomb scattering amplitude is not treated separately as in the elastic scattering channel.

Expressing $L' = L + K$ in the generalized NF decomposition (11), we obtain explicitly the near-side and far-side components of each K -subamplitude of the inelastic scattering amplitude (5) as

$$\begin{aligned} f_{M_{I'}}^{(K)}(\theta, \phi) &= f_{N, M_{I'}}^{(K)}(\theta, \phi) + f_{F, M_{I'}}^{(K)}(\theta, \phi) \\ &= \frac{\sqrt{4\pi}}{2ik} \sum_L \sqrt{2L+1} \langle (L+K) - M_{I'} I' M_{I'} | L0 \rangle \\ &\times A_{(L+K)M_{I'}} \exp[i(\sigma_L + \sigma'_{L+K} - M_{I'}\phi)] S'_{(L+K)L} \\ &\times \left[\tilde{Q}_{(L+K)-M_{I'}}^{(-)}(\cos\theta) + \tilde{Q}_{(L+K)-M_{I'}}^{(+)}(\cos\theta) \right]. \quad (12) \end{aligned}$$

Thus, the generalized NF decomposition (12) allows us to determine the near-side and far-side contributions from each K -subamplitude to the partial (7) and full inelastic cross section (8), and to study the formation of the nuclear rainbow in the inelastic nucleus-nucleus scattering in the same manner as done for the elastic scattering using the Fuller method (9).

3 Elastic and inelastic $^{12}\text{C}+^{12}\text{C}$ and $^{16}\text{O}+^{12}\text{C}$ scattering at the refractive energies

The diagonal matrix element $V_{\beta\beta}(R)$ of the projectile-target interaction in the CC equations (1) is determined by the total optical potential $U_0(R)$ [25]. The new version of the density dependent CDM3Y3 interaction with the rearrangement term included [24] is used in the double-folding calculation of the real optical potential $V_0(R)$. Because the nuclear rainbow is a subtle effect that can be observed only when the absorption of the dinuclear system is weak, the imaginary OP in the flexible Woods-Saxon (WS) form is usually used for a proper identification of the rainbow pattern. Thus, we have

$$\begin{aligned} U_0(R) &= N_R V_0(R) + iW_0(R) + V_C(R), \\ \text{where } W_0(R) &= -\frac{W_V}{1 + \exp[(R - R_V)/a_V]}. \quad (13) \end{aligned}$$

The Coulomb potential $V_C(R)$ is obtained by folding the two uniform charge distributions with their mean-squared radii chosen to be close to the measured charge radii of the two nuclei. The nuclear g.s. densities used in the DFM calculation are taken as the Fermi distributions with parameters chosen to reproduce the empirical matter radii of the considered nuclei [29]. The renormalization N_R of the real folded potential and the WS parameters (13) are adjusted in each case to the best CC description of the elastic scattering data, and a small deviation of N_R from unity validates the use of the folding model. The best-fit OP parameters used in the present CC study of the elastic and inelastic $^{12}\text{C}+^{12}\text{C}$ and $^{16}\text{O}+^{12}\text{C}$ scattering are given in Table 1.

The nondiagonal matrix element $V_{\beta\beta'}(R)$ in the CC equations (1) is given by the inelastic form factor $U_{I'}(R)$ that accounts for inelastic scattering to the target excited state with spin I' (see details in Ref. [25]),

$$U_{I'}(R) = N_R V_{I'}(R) - i\delta_{I'} \frac{\partial W_0(R)}{\partial R} + V_{C, I'}(R), \quad (14)$$

where the real nuclear $V_{I'}(R)$ and Coulomb $V_{C, I'}(R)$ inelastic form factors are calculated in the DFM using the nuclear transition densities of the excited states of ^{12}C obtained in the resonating group method (RGM) [30]. The nuclear deformation lengths $\delta_{I'}$ are determined by the collective-model prescription using the measured $B(EI')$ transition rates [31,32] of the considered excited states of ^{12}C . All the CC calculations have been done using the code ECIS97 written by Jacques Raynal [33] that provides the detailed output of the elastic and inelastic scattering

Table 1. The OP parameters (13) used in the CC calculation (1) of the elastic and inelastic $^{12}\text{C}+^{12}\text{C}$ and $^{16}\text{O}+^{12}\text{C}$ scattering. J_R and J_W are the volume integrals (per interacting nucleon pair) of the real and imaginary parts of the OP, respectively.

	E_{lab} (MeV)	N_R	J_R (MeV fm ³)	W_V (MeV)	R_V (fm)	a_V (fm)	J_W (MeV fm ³)	Data
$^{12}\text{C}+^{12}\text{C}$	240	1.067	336.0	19.29	5.743	0.595	117.5	[21, 22]
$^{16}\text{O}+^{12}\text{C}$	200	0.936	300.4	13.32	6.150	0.502	72.06	[16, 23]
$^{16}\text{O}+^{12}\text{C}$	260	0.930	291.8	18.50	5.756	0.550	83.92	[16, 23]

matrices necessary for the NF decomposition (9) and (12) of the corresponding scattering amplitudes. It should be recalled that the sequential iteration method implemented in the ECIS code was developed by Raynal to tackle the inelastic HI scattering with a strong Coulomb contribution, focusing in particular on the scattering experiments being carried out at GANIL at that time [34]. By using the recurrence relations for the Coulomb excitation integrals in the CC calculations [35], the ECIS integration of the coupled equations is highly stable and accurate up to very large radii with sufficiently high number of partial waves. For the $^{12}\text{C}+^{12}\text{C}$ and $^{16}\text{O}+^{12}\text{C}$ systems under the present study, the ECIS integration up to $R_{\text{max}} \approx 25$ fm in steps of $dR = 0.05$ fm is needed to ensure the convergence of the calculated cross section, taking into account up to 180 partial waves. At the considered energies, the CC results obtained using the nonrelativistic and relativistic kinematics are about the same.

The elastic and inelastic $^{12}\text{C}+^{12}\text{C}$ scattering has been widely studied at energies ranging from the Coulomb barrier [10] up to about 200 MeV/nucleon [36]. While the elastic $^{12}\text{C}+^{12}\text{C}$ scattering at the barrier energies was shown to be of interest for nuclear astrophysics [37], the scattering data measured for this system at the refractive energies around 20 MeV/nucleon [21, 22] exhibit a nuclear rainbow pattern that enabled an unambiguous determination of the real OP down to small distances [3, 24]. In particular, the $^{12}\text{C}+^{12}\text{C}$ scattering data measured accurately at $E_{\text{lab}} = 240$ MeV [21, 22] are very important for our study because this energy was found optimal for the observation of the first Airy minimum A1 of the nuclear rainbow in the elastic $^{12}\text{C}+^{12}\text{C}$ scattering [24]. As shown above in Fig. 1, the data of the inelastic $^{12}\text{C}+^{12}\text{C}$ scattering to the 2_1^+ (4.44 MeV) state of ^{12}C measured at this same energy [21, 22] does not have any minimum that can be interpreted as the remnant of A1, at angles near the location of A1 established in the elastic cross section. Another light HI system that exhibits a prominent rainbow pattern in the elastic scattering is $^{16}\text{O}+^{12}\text{C}$ [23]. Unlike $^{12}\text{C}+^{12}\text{C}$, the $^{16}\text{O}+^{12}\text{C}$ system does not have the boson symmetry, and the angular evolution of the Airy pattern could be observed with the increasing energy. The strongest rainbow pattern, the deep A1 minimum followed by an exponential fall-off of the rainbow shoulder, is well confirmed in the elastic $^{16}\text{O}+^{12}\text{C}$ scattering data measured at $E_{\text{lab}} = 200$ MeV [23]. The question why the inelastic $^{16}\text{O}+^{12}\text{C}$ scattering data measured at this same energy [16] does not show a similar Airy pattern (see lower panel of Fig. 1) is so far unanswered. In the present work, we try to explain

the suppression of the first Airy minimum in the inelastic $^{12}\text{C}+^{12}\text{C}$ and $^{16}\text{O}+^{12}\text{C}$ scattering cross sections at the energies where A1 was clearly identified in the elastic cross sections measured for these systems.

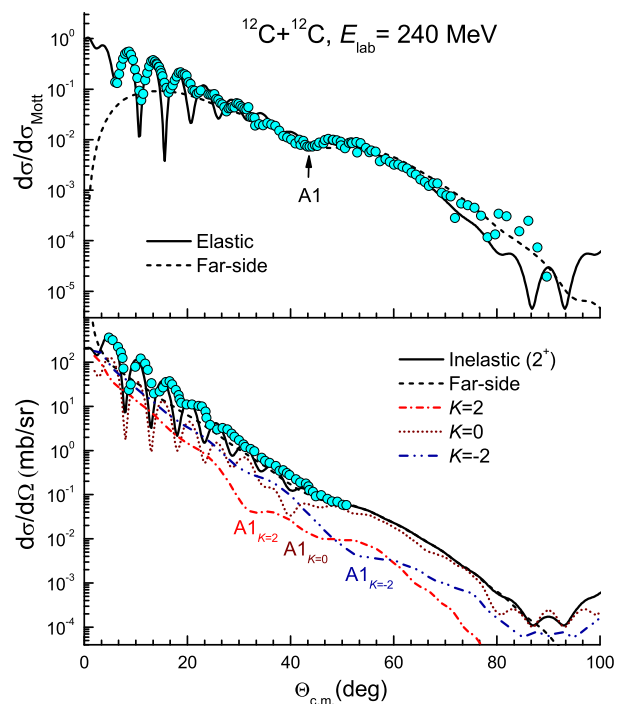


Fig. 2. CC description (solid lines) of the elastic and inelastic (to the 2_1^+ state of ^{12}C) $^{12}\text{C}+^{12}\text{C}$ scattering at $E_{\text{lab}} = 240$ MeV, in comparison with the measured data [21, 22]. The dash-dotted, dotted, and dash-dot-dotted lines are the partial inelastic cross sections (7) given by the subamplitudes with $K = 2, 0$ and -2 , respectively. The dashed lines are the far-side cross sections given by the NF decompositions (9) and (11) of the elastic and inelastic scattering amplitudes. The first Airy minimum A1 is shown explicitly for each partial inelastic cross section.

The CC results for the elastic and inelastic $^{12}\text{C}+^{12}\text{C}$ scattering describe well the data as shown in Fig. 2. The dominance of the far-side cross sections at medium and large angles indicates that both the elastic- and inelastic $^{12}\text{C}+^{12}\text{C}$ at the considered energies are strongly refractive. The nuclear rainbow pattern is well established in the elastic $^{12}\text{C}+^{12}\text{C}$ scattering, with the first Airy minimum A1 unambiguously identified [24] at the scattering angle $\theta_{\text{c.m.}} \approx 41^\circ$ based on the NF decomposition (9) of

the elastic scattering amplitude. The data of the inelastic $^{12}\text{C}+^{12}\text{C}$ scattering to the 2_1^+ state of ^{12}C are reproduced reasonably by the CC calculation (1), but the Airy structure seen in the elastic cross section is smeared out in the inelastic cross section. Given the dominance of the far-side scattering at medium and large angles, the suppression of A1 in the inelastic cross section is definitely *not* caused by the near-side/far-side interference, but more likely by a destructive interference of the far-side subamplitudes.

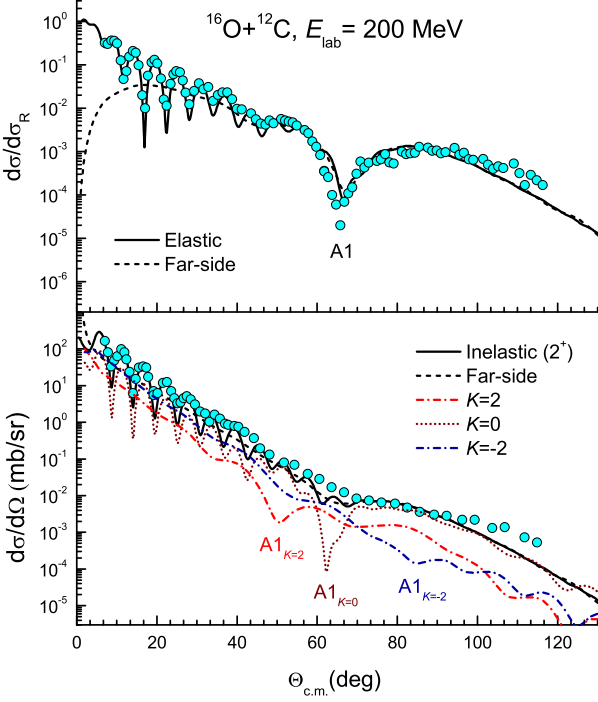


Fig. 3. The same as Fig. 2 but for the elastic and inelastic $^{16}\text{O}+^{12}\text{C}$ scattering at $E_{\text{lab}} = 200$ MeV [16, 23].

One can see in the partial-wave expansion of the inelastic scattering amplitude (3) that the inelastic scattering cross section at the given scattering angle contains the contributions from the subamplitudes of different partial waves ($L' \neq L$) when the spin of the excited state is nonzero ($I' \neq 0$). For the inelastic $^{12}\text{C}+^{12}\text{C}$ scattering to the 2_1^+ state of ^{12}C shown in Fig. 2, each L -component of the inelastic scattering amplitude is resulting from an interference of the three K -subamplitudes with $K = L' - L = -2, 0, 2$. The partial inelastic scattering cross sections (7) given by the three K -subamplitudes (summed over all partial waves L) are shown separately in the lower panel of Fig. 2. By tracing the angular evolution of the corresponding far-side cross sections, we have identified the first Airy minimum A1 in the partial inelastic $^{12}\text{C}+^{12}\text{C}$ cross section with $K = 0$ at $\theta_{\text{c.m.}} \approx 40^\circ$ which is close to the locations of A1 in the elastic $^{12}\text{C}+^{12}\text{C}$ cross section. While a slight remnant of A1 with $K = 0$ can still be seen in the calculated inelastic scattering cross section (8), it is not observed in the measured data. Rather weak rainbow patterns of the two partial inelastic $^{12}\text{C}+^{12}\text{C}$ cross sections

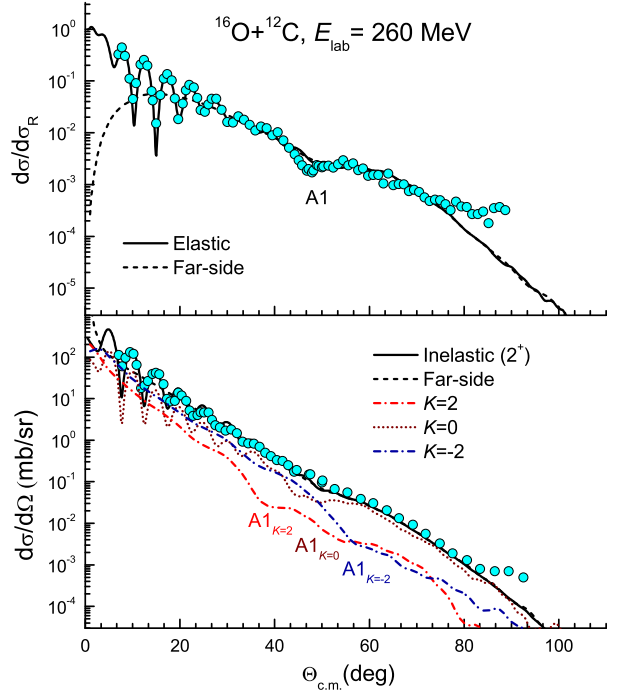


Fig. 4. The same as Fig. 2 but for the elastic and inelastic $^{16}\text{O}+^{12}\text{C}$ scattering at $E_{\text{lab}} = 260$ MeV [16, 23].

with $K \neq 0$ were found which are shifted in angles, with A1 located at $\theta_{\text{c.m.}} \approx 33^\circ$ and 52° in the partial inelastic cross section with $K = 2$ and $K = -2$, respectively. One can see in the lower panel of Fig. 2 that the partial inelastic cross sections with $K = \pm 2$ are much weaker than that with $K = 0$ at medium and large angles, and no remnants of A1 with $K = \pm 2$ can be seen in the total inelastic cross section.

A similar picture can be seen in the CC results for the elastic and inelastic $^{16}\text{O}+^{12}\text{C}$ scattering at $E_{\text{lab}} = 200$ MeV plotted in Fig. 3. While the prominent A1 minimum is located at $\theta_{\text{c.m.}} \approx 65^\circ$ in the elastic cross section, it seems to disappear in the inelastic $^{16}\text{O}+^{12}\text{C}$ scattering cross section. Such an effect was found also in the results of the earlier CC analysis of the inelastic $^{16}\text{O}+^{12}\text{C}$ scattering [38] as well as those of a cluster folded model study [39]. As discussed for the $^{12}\text{C}+^{12}\text{C}$ system, three different Airy oscillation patterns can be seen in the partial inelastic $^{16}\text{O}+^{12}\text{C}$ cross sections given by the subamplitudes with $K = 2, 0, -2$, with A1 located at $\theta_{\text{c.m.}} \approx 49^\circ, 62^\circ$, and 84° , respectively. Again, the location of A1 with $K = 0$ is quite close to the locations of A1 in the elastic $^{16}\text{O}+^{12}\text{C}$ cross section. The full inelastic scattering cross section (8) includes the contributions from all allowed K -subamplitudes, and their out-of-phase interference smears out the individual A1 minima seen in the partial inelastic cross sections (7). While a slight remnant of A1 with $K = 0$ is seen in the calculated inelastic cross section (solid line in the lower panel of Fig. 3), it cannot be clearly resolved in the measured data. The same CC results for the elastic and inelastic $^{16}\text{O}+^{12}\text{C}$ scat-

tering at $E_{\text{lab}} = 260$ MeV are compared with the data [16, 23] in Fig. 4. We found that the absorption becomes slightly stronger (see Table 1) with the increasing energy, and the Airy oscillation pattern is weakened and shifted to smaller angles (with A1 in the elastic cross section located at $\theta_{\text{c.m.}} \approx 50^\circ$). The weaker Airy oscillation pattern of each partial inelastic cross section can still be seen but the remnant of A1 with $K = 0$ disappears in both the calculated inelastic scattering cross section and measured data (lower panel of Fig. 4). In conclusion, the results of our CC analysis shown in Figs. 2-4 explain naturally why the Airy oscillation pattern of the nuclear rainbow is strongly suppressed in the measured data of the inelastic $^{12}\text{C}+^{12}\text{C}$ and $^{16}\text{O}+^{12}\text{C}$ scattering to the 2_1^+ state of ^{12}C at the rainbow energies.

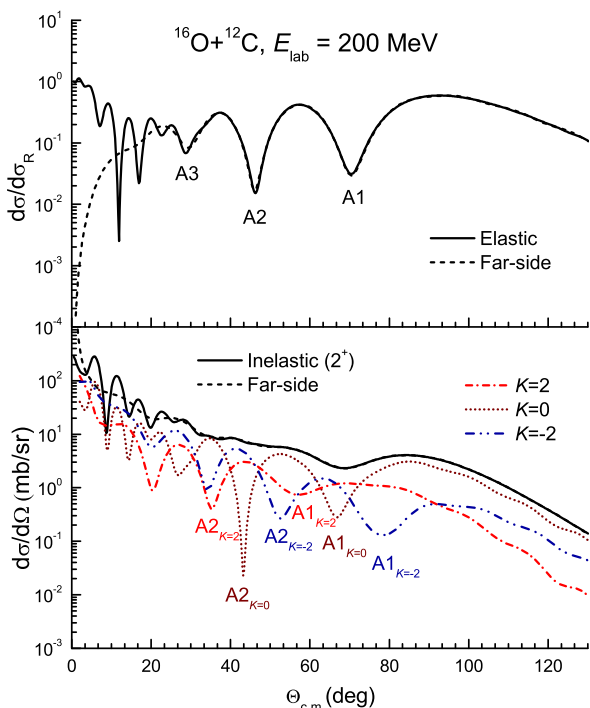


Fig. 5. The same CC results as those in Fig. 3 for the elastic and inelastic $^{16}\text{O}+^{12}\text{C}$ scattering at $E_{\text{lab}} = 200$ MeV, obtained with a less absorptive OP (13) with $W_V \rightarrow W_V/3$.

It is well-known that the nuclear rainbow is formed by the interference of the far-side scattering waves, refracted by the attractive *real* OP [2, 3]. That's the reason why the nuclear rainbow could be observed only when the absorption of the scattering system is weak enough for the far-side trajectories to survive at the medium and large scattering angles. In practice, the absorptive strength of the OP is often reduced to artificially enhance the far-side scattering amplitude for a proper identification of the Airy oscillation pattern [24]. The results of the CC calculation of the elastic and inelastic $^{16}\text{O}+^{12}\text{C}$ scattering at 200 MeV given by a less absorptive OP (with $W_V \rightarrow W_V/3$) are plotted in Fig. 5, and one can trace in the elastic cross section the whole pattern of the nuclear rainbow including

the first (A1), second (A2), and third (A3) Airy minima. The same Airy oscillation pattern can be seen also in the three partial inelastic scattering cross sections (7) given by the three K -subamplitudes (6), but the locations of the Airy minima are shifted to the smaller angles when $K = 2$, and to the larger angles when $K = -2$. It is very essential to emphasize again that the Airy oscillation pattern in the partial inelastic cross section with $K = 0$ remains about the same as that observed in the elastic scattering thanks to an in-phase interference of the partial waves with $L' = L$. When $K \neq 0$, the out-of-phase interference of the partial waves with $L' \neq L$ smears out the different Airy oscillation patterns in the full inelastic 2_1^+ scattering cross section. Because the partial inelastic cross section with $K = 0$ is substantially larger than those with $K = \pm 2$ at medium and large angles, the remnant of the first Airy minimum A1 with $K = 0$ can be very well seen in the full inelastic scattering cross section (solid line in the lower panel of Fig. 5) when a reduced absorption W_V was used in the CC calculation. In fact, the broad rainbow shoulder following A1 with $K = 0$ is still visible in the data measured at $E_{\text{lab}} = 200$ MeV for the inelastic $^{16}\text{O}+^{12}\text{C}$ scattering to the 2_1^+ state of ^{12}C (see lower panel of Fig. 3).

It becomes clear now that there is no unique Airy pattern of the nuclear rainbow in the full (far-side) cross section of the inelastic nucleus-nucleus scattering to an excited nuclear state with nonzero spin. In such a case, only the Airy oscillation pattern of the partial inelastic cross section (7) given separately by each K -subamplitude (6) can be determined in the same manner as done in the case of elastic scattering. Thus, the detailed locations of the Airy minima A1, A2, and A3 in the inelastic $^{16}\text{O}+^{12}\text{C}$ scattering cross section deduced visually by Ohkubo *et al.* from the calculated angular distribution [38] are not properly founded.

Although the inelastic $^{16}\text{O}+^{12}\text{C}$ scattering to the 0_2^+ (Hoyle) and 3_1^- excited states (at $E_x \approx 7.65$ and 9.64 MeV, respectively) were not measured at $E_{\text{lab}} = 200$ MeV, the CC prediction of the inelastic cross sections for these states should be of interest for the revelation of the nuclear rainbow pattern therein. The CC results for the inelastic $^{16}\text{O}+^{12}\text{C}$ scattering at 200 MeV obtained with the nuclear transition densities of the 0_2^+ and 3_1^- states of ^{12}C given by the RGM [30] and the same OP as given in Table 1 are shown in Fig. 6. One can see that the refractive (far-side) scattering is also dominant at medium and large angles in the inelastic scattering to the Hoyle (0_2^+) state, with $K \equiv 0$ (or $L' \equiv L$) and $d\sigma_K/d\Omega \equiv d\sigma/d\Omega$. In this case, spin of the excited state is zero and there is no interference of the scattering subamplitudes with different K . As a result, the Airy pattern in the angular distribution of the inelastic scattering to the Hoyle state is determined with a single ($K = 0$) inelastic scattering amplitude, in the same manner as done for the elastic $^{16}\text{O}+^{12}\text{C}$ scattering. Thus, the deep minimum of the inelastic 0_2^+ cross section can be confirmed as the first Airy minimum A1 which is located at about the same angle as A1 of the elastic cross section (see upper panels of Figs. 5 and 6).

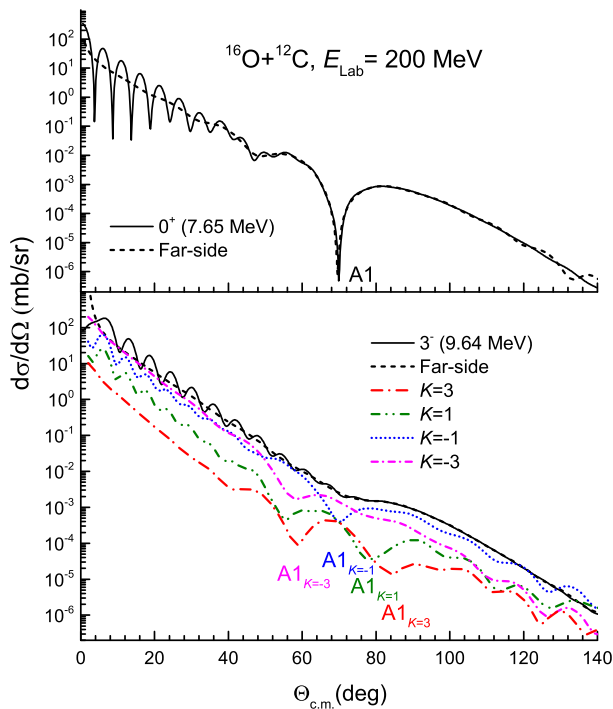


Fig. 6. The same CC results as those in Fig. 2 but for the inelastic $^{16}\text{O}+^{12}\text{C}$ scattering to the 0_2^+ (upper part) and 3_1^- (lower part) excited states of ^{16}O at $E_{\text{lab}} = 200$ MeV.

For the inelastic $^{16}\text{O}+^{12}\text{C}$ scattering to the 3_1^- state of ^{12}C , there are four subamplitudes (6) with $K = -3$ ($L' = L - 3$), $K = -1$ ($L' = L - 1$), $K = 1$ ($L' = L + 1$), and $K = 3$ ($L' = L + 3$) with the corresponding A1 minima shifted away from each other by a few degrees in the scattering angle. Among these K -subamplitudes, The first Airy minimum A1 of the partial inelastic cross section with $K = -1$ is quite pronounced. One can see in the lower panel of Fig. 6 that the out-of-phase interference of these 4 subamplitudes results in a rather smooth full inelastic scattering cross section (8). This is the same effect of suppression of the Airy pattern as discussed above for the inelastic $^{16}\text{O}+^{12}\text{C}$ scattering to the 2_1^+ state of ^{12}C .

4 Summary

The present work explains why the Airy pattern of nuclear rainbow is suppressed in the inelastic $^{12}\text{C}+^{12}\text{C}$ and $^{16}\text{O}+^{12}\text{C}$ scattering to the 2_1^+ state of ^{12}C at the refractive energies, where a strong rainbow pattern has been observed in the elastic scattering. For this purpose, the near-far decomposition method by Fuller is generalized to determine the near-side and far-side components of the inelastic scattering amplitude for all partial wave contributions. Using the generalized NF decomposition method, our coupled channel analysis of the elastic and inelastic $^{12}\text{C}+^{12}\text{C}$ and $^{16}\text{O}+^{12}\text{C}$ scattering at the energies under study shows unambiguously that the destructive interference of the inelastic partial waves of different multipoles

suppresses the Airy oscillation pattern in the inelastic scattering cross section. Nevertheless, the inelastic scattering remains strongly refractive in these cases, with the dominant far-side scattering at medium and large scattering angles.

We conclude, therefore, that it is not possible to identify uniquely the Airy pattern of the nuclear rainbow in the angular distribution of the inelastic nucleus-nucleus scattering to an excited state with nonzero spin. Semi-classically, such a refractive mixing of the partial waves of different multipoles is analogous to an optical prism refracting ray of light of different wave lengths. The only exception is the inelastic scattering to a monopole excitation which does not mix different multipoles in the inelastic scattering amplitude, and the Airy pattern in the inelastic cross section can be determined consistently in the same manner as done for the elastic scattering. In light of this result, an accurate measurement of the inelastic α or light ion scattering to the 0_2^+ excitation of the ^{12}C target should be of interest for the future studies of the nuclear rainbow scattering as well as the α -cluster structure of the Hoyle state [40, 41].

Last but not least, we gratefully notice that over the years our nuclear scattering study has been relied on several versions of the coupled channel code ECIS written by Jacques Raynal. This state-of-the-art computer code of nuclear scattering is still being actively used in the community, and Jacques' important contribution to the development of the nuclear physics research is strongly appreciated by many of us.

Acknowledgments

The present research was supported, in part, by the National Foundation for Science and Technology Development (NAFOSTED). The authors also thank Prof. M. Kamimura for his permission to use the RGM nuclear densities in the double-folding calculation.

References

1. M.E. Brandan, M.S. Hussein, K.W. McVoy, and G.R. Satchler, *Comments on nuclear and particle physics*, Vol. 22 (Gordon and Breach, New York, 1996), p. 77.
2. M.E. Brandan and G.R. Satchler, *Phys. Rep.* **285**, 143 (1997).
3. D.T. Khoa, W. von Oertzen, H.G. Bohlen, and S. Ohkubo, *J. Phys. G* **34**, R111 (2007).
4. F. Michel, G. Reidemeister, and S. Ohkubo, *Phys. Rev. C* **61**, 041601 (2000).
5. S. Ohkubo, *Phys. Rev. C* **93**, 041303 (2016).
6. D.M. Brink and N. Takigawa, *Nucl. Phys. A* **279**, 159 (1977).
7. R.C. Fuller, *Phys. Rev. C* **12**, 1561 (1975).
8. F. Michel, F. Brau, G. Reidemeister, and S. Ohkubo, *Phys. Rev. Lett.* **85**, 1823 (2000).
9. R. Anni, *Phys. Rev. C* **63**, 031601 (2001).
10. N. Rowley, H. Doubre, and C. Marty, *Phys. Lett. B* **69**, 147 (1977).

11. H.G. Bohlen, M.R. Clover, G. Ingold, H. Lettau, and W. von Oertzen, *Z. Phys. A* **308**, 121 (1982).
12. D.T. Khoa and O.M. Knyazkov, *Z. Phys. A* **328**, 67 (1987).
13. D.T. Khoa, H. Bohlen, W. von Oertzen, G. Bartnitzky, A. Blazevic, F. Nuoffer, B. Gebauer, W. Mittig, and P. Roussel-Chomaz, *Nucl. Phys. A* **759**, 3 (2005).
14. F. Michel and S. Ohkubo, *Phys. Rev. C* **70**, 044609 (2004).
15. S. Hamada, Y. Hirabayashi, N. Burtebayev, and S. Ohkubo, *Phys. Rev. C* **87**, 024311 (2013).
16. S. Ohkubo, Y. Hirabayashi, A.A. Ogloblin, Y.A. Glukhov, A.S. Dem'yanova, and W.H. Trzaska, *Phys. Rev. C* **90**, 064617 (2014).
17. A. Dem'yanova, V. Bragin, A. Ogloblin, A. Lebedev, J. Bang, S. Goncharov, S. Ershov, F. Gareev, and P. Korovin, *Physics Letters B* **184**, 129 (1987).
18. A. Dem'yanova, E. Svinareva, S. Goncharov, S. Ershov, F. Gareev, G. Kazacha, A. Ogloblin, and J. Vaagen, *Nucl. Phys. A* **542**, 208 (1992).
19. A. D'Arrigo, G. Fazio, G. Giardina, O. Goryunov, A. Ilyin, M. Sacchi, A. Shvedov, A. Taccone, I. Vishnevsky, and I. Zaiats, *Il Nuovo Cimento A* **107**, 1353 (1994).
20. P. D'Agostino, G. Fazio, G. Giardina, O. Goryunov, M. Sacchi, A. Shvedov, I. Vishnevsky, and I. Zaiatz, *Nucl. Phys. A* **583**, 437 (1995).
21. H. Bohlen, X. Chen, J. Cramer, P. Frobrich, B. Gebauer, H. Lettau, A. Miczaika, W. von Oertzen, R. Ulrich, and T. Wilpert, *Z. Phys. A* **322**, 241 (1985).
22. A. Dem'yanova, H. Bohlen, A. Danilov, S. Goncharov, S. Khlebnikov, V. Maslov, Y. Penionzkevich, Y. Sobolev, W. Trzaska, G. Tyurin, and A. Ogloblin, *Nucl. Phys. A* **834**, 473c (2010).
23. A.A. Ogloblin, Y.A. Glukhov, W.H. Trzaska, A.S. Dem'yanova, S.A. Goncharov, R. Julin, S.V. Klebnikov, M. Mutterer, M.V. Rozhkov, V.P. Rudakov, G.P. Tiorin, D.T. Khoa, and G.R. Satchler, *Phys. Rev. C* **62**, 044601 (2000).
24. D.T. Khoa, N.H. Phuc, D.T. Loan, and B.M. Loc, *Phys. Rev. C* **94**, 034612 (2016).
25. D.T. Khoa and G. Satchler, *Nucl. Phys. A* **668**, 3 (2000).
26. G. Satchler, *Direct Nuclear Reactions* (Clarendon, Oxford, 1983).
27. K.W. McVoy and M.E. Brandan, *Nucl. Phys. A* **542**, 295 (1992).
28. D.R. Dean and N. Rowley, *J. Phys. G* **10**, 493 (1984).
29. D.T. Khoa, *Phys. Rev. C* **63**, 034007 (2001).
30. M. Kamimura, *Nuclear Physics A* **351**, 456 (1981).
31. S. Raman, C. Malarkey, W. Milner, C. Nestor, and P. Stelson, *Atomic Data and Nuclear Data Tables* **36**, 1 (1987).
32. T. Kibédi and R. Spear, *Atomic Data and Nuclear Data Tables* **80**, 35 (2002).
33. J. Raynal, *Computing as a Language of Physics* (IAEA, Vienna, 1972) p. 75; J. Raynal, coupled-channel code ECIS97 (unpublished).
34. N. Alamanos, *Eur. Phys. J. A* **56**:212, (2020).
35. J. Raynal, *Phys. Rev. C* **23**, 2571 (1981).
36. J. Hostachy, M. Buenerd, J. Chauvin, D. Lebrun, P. Martin, J. Lugol, L. Papineau, P. Roussel, N. Alamanos, J. Arvieux, and C. Cerruti, *Nucl. Phys. A* **490**, 441 (1988).
37. L.H. Chien, D.T. Khoa, D.C. Cuong, and N.H. Phuc, *Phys. Rev. C* **98**, 064604 (2018).
38. S. Ohkubo, Y. Hirabayashi, and A.A. Ogloblin, *Phys. Rev. C* **96**, 024607 (2017).
39. M.A. Hassanain, F.M.Z. Alqahtani, A.A. Ibraheem, M. Anwar, K.O. Behary, Z.M. Mahmoud, and M. El-Azab Farid, *Phys. Rev. C* **98**, 014621 (2018).
40. D.T. Khoa and D.C. Cuong, *Phys. Lett. B* **660**, 331 (2008).
41. S. Ohkubo and Y. Hirabayashi, *Phys. Rev. C* **70**, 041602 (2004).

